

Applications of nanostructures in wide-field, label-free super resolution microscopy

XiaoWei Liu(刘小威), Chao Meng(孟超), XueChu Xu(徐雪初), MingWei Tang(汤明炜), ChenLei Pang(庞陈雷), Qing Yang(杨青)

Citation: Chin. Phys. B . 2018, 27(11): 118704. **doi:** 10.1088/1674-1056/27/118704
Journal homepage: http://cpb.iphy.ac.cn; http://iopscience.iop.org/cpb

What follows is a list of articles you may be interested in

Controlling flexural waves in thin plates by using transformation acoustic metamaterials

Xing Chen(陈幸), Li Cai(蔡力), Ji-Hong Wen(温激鸿)
Chin. Phys. B . 2018, 27(5): 057803. **doi:** 10.1088/1674-1056/27/5/057803

Investigation of noise properties in grating-based x-ray phase tomography with reverse projection method

Bao Yuan, Wang Yan, Gao Kun, Wang Zhi-Li, Zhu Pei-Ping, Wu Zi-Yu
Chin. Phys. B . 2015, 24(10): 108702. **doi:** 10.1088/1674-1056/24/10/108702

Terahertz plasmon and surface-plasmon modes in cylindrical metallic nanowires

Wu Ping, Xu Wen, Li Long-Long, Lu Tie-Cheng, Wu Wei-Dong
Chin. Phys. B . 2014, 23(10): 107807. **doi:** 10.1088/1674-1056/23/10/107807

An effective surface-enhanced Raman scattering template based on gold nanoparticle/silicon nanowire arrays

Wang Ming-Li, Zhang Chang-Xing, Wu Zheng-Long, Jing Xi-Li, Xu Hai-Jun
Chin. Phys. B . 2014, 23(6): 067802. **doi:** 10.1088/1674-1056/23/6/067802

Influence of polarization direction, incidence angle, and geometry on near-field enhancement in two-layered gold nanowires

Wu Da-Jian, Jiang Shu-Min, Liu Xiao-Jun
Chin. Phys. B . 2012, 21(7): 077803. **doi:** 10.1088/1674-1056/21/7/077803

TOPICAL REVIEW — Nanolasers

Applications of nanostructures in wide-field, label-free super resolution microscopy*

Xiaowei Liu(刘小威), Chao Meng(孟超), Xuechu Xu(徐雪初), Mingwei Tang(汤明炜), Chenlei Pang(庞陈雷), and Qing Yang(杨青)†

State Key Laboratory of Modern Optical Instrumentation, College of Optical Science and Engineering, Zhejiang University, Hangzhou 310027, *China*

(Received 11 June 2018; revised manuscript received 31 August 2018; published online 19 October 2018)

Super resolution imaging capable of resolving details beyond the diffraction limit is highly desired in many scientific and application fields, including bio-medicine, nanomaterial science, and opto-electronic integration. Up to now, many different methods have been proposed, among which wide-field, label-free super resolution microscopy is indispensable due to its good applicability to diverse sample types, large field of view (FOV), and high imaging speed. In recent years, nanostructures have made a crucial contribution to the wide-field, label-free subdiffraction microscopy, with various working mechanisms and configuration designs. This review summarizes the recent applications of the nanostructures in the wide-field, label-free super resolution microscopy, with the emphasis on the designs of hyperlens with hyperbolic dispersion, microsphere with "nano-jets", and nanowire ring illumination microscopy based on spatial frequency shift effect. The bottlenecks of the current techniques and possible solutions are also discussed.

Keywords: optical microscopy, spatial resolution, nanowire, metamaterials

PACS: 87.64.M–, 87.57.cf, 78.67.Uh, 78.67.Pt **DOI:** 10.1088/1674-1056/27/11/118704

1. Introduction

Optical microscopy techniques with high resolution play a primary role in the development or even revolution in many important areas, such as biomedicine, life science, and material science, by expanding our view of objects into micro or even nanoscale, which is too small to be seen with the naked eye. However, in classical microcopy systems, the physical resolution is limited to $\sim 0.5\lambda/\mathrm{NA}$ due to the diffraction of light, where λ is the wavelength of light and NA is the numerical aperture. Super resolution imaging capable of resolving details beyond the diffraction limit is of great significance and thus has attracted worldwide research interest. In recent decades, great improvement in the resolution of optical microscopy has been achieved through different approaches.[1–7] In general, subdiffraction microscopy can be divided into two groups: (i) label based subdiffraction microscopy (the sample is labelled by fluorescent molecules and the signal comes from the fluorescence of the chromophore); and (ii) label-free subdiffraction microscopy. The label based subdiffraction imaging techniques develop much faster than the label-free ones, and in 2014 the Nobel Prize in Chemistry was awarded to Eric Betzig, Stefan W. Hell, and William E. Moerner for the development of super-resolved fluorescence microscopy.[8–14] However, the long preprocessing and high selectivity of chromophores make these techniques difficult to use to image an abiological specimen. Meanwhile, the rapid advances in nano-optics, nano-electronics, material science, and so on have made stringent demand for label-free super resolution microscopy. To realize the label-free super resolution microscopy, the subdiffraction spatial frequency information should be incorporated into the final image construction, which is carried by the near-field evanescent waves and thus cannot be captured by the classical imaging system. A straightforward way to capture the subdiffraction spatial frequency information is to use an ultrathin nano-tip to detect the near-field signal at the very surface of the sample;[15,16] that is, the near-field scanning optical microscopy (SNOM). Nevertheless, major drawbacks of this technique include the low imaging speed that results from the scanning process, and the sophisticated control of the distance between the tip and the surface of the objects in every pixel. Therefore, developing a brand-new wide-field, label-free super resolution microscopy with high imaging speed and large field of view (FOV) has become a popular area of research.

To realize label-free, wide-field super resolution imaging, it is essential to realize light–matter interaction in the near-field within a wide area, and to then transfer the evanescent waves carrying subdiffraction spatial frequency information to propagating waves that can be detected by a conventional wide-field imaging system.

*Project supported by the National Natural Science Foundation of China (Grant Nos. 61735017 and 51672245), the Zhejiang Provincial Natural Science Foundation of China (Grant No. R17F050003), the National Key Basic Research Program of China (Grant No. 2015CB352003), the Fundamental Research Funds for the Central Universities, China, the Program for Zhejiang Leading Team of S&T Innovation, China, the Cao Guangbiao Advanced Technology Program, China, and First-class Universities and Academic Programs, China.

†Corresponding author. E-mail: qingyang@zju.edu.cn

© 2018 Chinese Physical Society and IOP Publishing Ltd

Nanostructures have shown great potential in generating or interacting with the evanescent waves with high efficiency due to their unique optical properties, strong spatial light localization,[17,18] high aspect ratio,[19,20] high refractive index,[21] and small footprint, thus becoming a good candidate for achieving the wide-field, label-free super resolution microscopy. Recent studies of the applications of nanostructures (e.g., hyperlens, microspheres, and fluorescent nanowire ring (NWR) illumination) in the wide-field, label-free super resolution microscopy have demonstrated great improvement in the available FOV, resolution, and versatility. In this paper, we will review the research progress in nanostructures based super resolution microscopy.

2. Nanostructures based wide-field, label-free, super-resolution imaging

2.1. Hyperlens with hyperbolic dispersion

The dispersion relation of propagating electromagnetic (EM) wave in an ordinary medium with positive refractive index can be represented by a curve of circle or ellipse (the discussion is conducted in two-dimensional case for simplification), in which the increase of one component of the wave vector causes the other component to decrease. In particular, when one component exceeds the range covered by the dispersion curve, the other component would become a purely imaginary number, resulting in exponentially decaying EM wave along the corresponding direction; that is, evanescent wave. Consequently, the high spatial frequency information which represents the subdiffraction details of an object is carried by the evanescent wave and cannot be delivered to the far field, which leads to the diffraction limited resolution.

To overcome this limitation, researchers resort to the anisotropic medium that possesses dielectric permittivities of different signs along different directions (metamaterial). In this condition, the dispersion relation curve changes from elliptical to hyperbolic shape and allows the propagating of the waves with much larger wave vectors to carry subdiffraction spatial frequency information of the object. A cylindrical structure with a hollow core was proposed to enable the waves carrying subdiffraction spatial information to propagate after they have departed from this special medium and thus achieve a real far-field imaging.[22] Its dispersion relation is given as follows:

$$\frac{k_r^2}{\varepsilon_\theta} + \frac{k_\theta^2}{\varepsilon_r} = \frac{\omega^2}{c^2}, \tag{1}$$

where ε_θ and ε_r denote the tangential and radial dielectric permittivity ($\varepsilon_\theta > 0$, $\varepsilon_r < 0$), and k_θ and k_r are the tangential and radial wave vectors, respectively. The light scattered or emitted by the object placed at the inner cylindrical surface stimulates a wide range of k_θ. During the propagation, k_θ gradually decreases due to the conservation of the angular momentum. Finally, the subdiffraction features can be carried by the light of small k_θ that enters into the surrounding ordinary medium as propagating waves for the far-field, wide-field detection. The super resolution imaging process can also be understood in real space as the process that the subdiffraction object is gradually magnified by the hyperlens to a scale that can be resolved by a far-field conventional imaging system.

This cylindrical medium with hyperbolic dispersion is called a hyperlens. Since metals tend to have negative dielectric permittivity and dielectrics have positive dielectric permittivity in the visible frequency range, metamaterials which contain both of the materials can be designed to exhibit the expected opposite signs of permittivity in two orthogonal directions.[22] Metals and dielectrics are fabricated as deep subwavelength layers for effective medium approximation. In 2007, Liu *et al.* first experimentally demonstrated a magnified optical hyperlens consisting of a curved periodic stack of Ag (35 nm) and Al_2O_3 (35 nm) deposited on half a cylindrical cavity fabricated on a quartz substrate[23] as shown in Fig. 1(a). In their results, a one-dimensional line-pair with 150 nm in spacing was resolved (Fig. 1(b)) at 365 nm ultraviolet wavelength with a 1.4 NA objective. The structure was magnified by the cylindrical hyperlens to a size beyond the diffraction limited resolution of the conventional objective ($\lambda/\mathrm{NA} \sim 260$ nm).

The concentric multilayered hyperlens can only work in the UV spectrum range because the wavelengths are strictly limited within the UV range to achieve a negative permittivity along the layer ($\varepsilon_\parallel$) and at the same time a positive permittivity normal to the layers ($\varepsilon_\perp$). Moreover, the resonant nature of the negative $\varepsilon_\parallel$ response causes high loss. In 2015, Sun *et al.* reported a non-resonant radial fan-shaped hyperlens with positive $\varepsilon_\parallel$, while negative $\varepsilon_\perp$ can also achieve a hyperbolic dispersion curve such as that in Ref. [23] but works in a visible spectrum range and with much lower loss.[24] A fan-shaped structure is more difficult to fabricate than a concentric multilayered device. Their fan-pattern was fabricated in a PMMA film waveguide by electron beam lithography (EBL) and then was electroplated with gold. The schematic diagram of the hyperlens is shown in Fig. 2(a). The incident light propagates in the film waveguide, and encounters the objects etched in the film. The scattered light transmits through the downstream hyperlens and is then coupled out from the film waveguide by an arc-shaped port to a far-field imaging system. Figure 2(b) shows the SEM image of the top view of the entire structure. Figure 2(c) shows the experimental result of imaging a diffraction limited object consisting of two 80-nm-wide slits with 250 nm in spacing (860 nm effective wavelength).

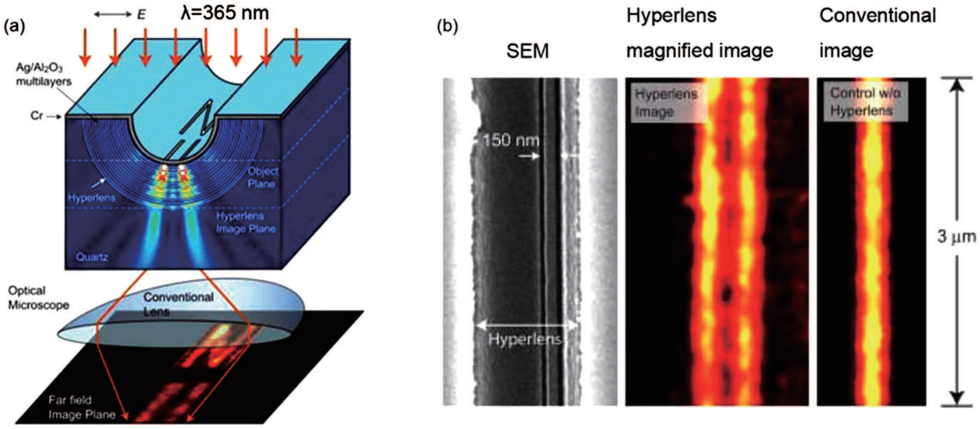


Fig. 1. (color online) Multilayered cylindrical hyperlens. (a) Schematic of hyperlens and numerical simulation of imaging of sub-diffraction-limited object. (b) Hyperlens imaging of an object (a pair of lines with spacing of 150 nm). From left to right, scanning electron microscope (SEM) image of a line-pair object fabricated near inner side of hyperlens, magnified hyperlens image showing that 150-nm-spaced line-pair object can be clearly resolved, and resulting diffraction-limited image from control experiment without hyperlens. The hyperlens that is used is comprised of 16 layers of Ag/Al_2O_3. Reproduced with permission from Ref. [23].

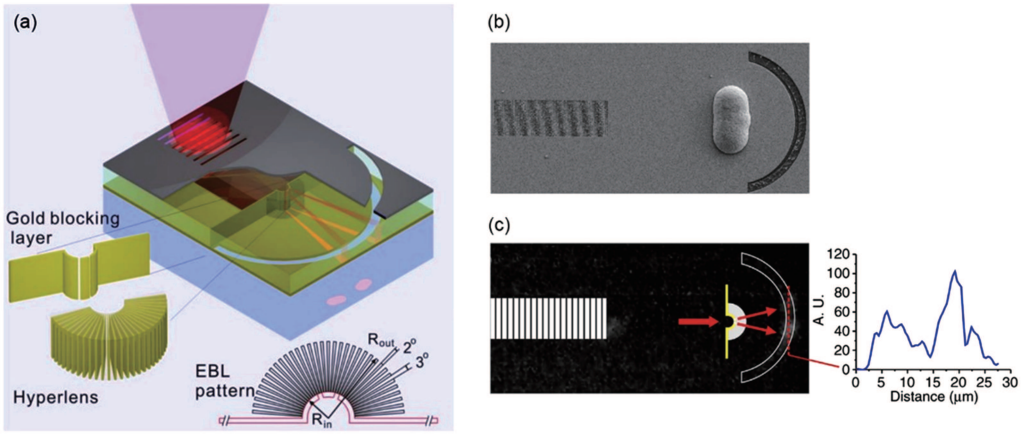


Fig. 2. (color online) Optical fan-shaped hyperlens with radial layered structures. (a) Schematic of waveguide-integrated fan-shaped hyperlens, with inset showing hyperlens and blocking layer with two nano-slits that serve as object to be imaged. (b) SEM image of entire sample with hyperlens. On the left-hand is a grating coupler that is used as input port, and on the right-hand is the output port, which is an arc-shaped slit. The hyperlens is shown to be between the grating coupler and the curved slit. The capsule shaped protuberant ridge is excess gold that has expanded out of PMMA structure during electroplating. (c) Direct visualization at output port taken by using CCD camera. Panel on the right side shows profile of output beams. Reproduced with permission from Ref. [24].

The cylindrical hyperlens has previously been investigated and promoted, and the results can be found in Refs. [25]–[29], although most of those results were limited to one-dimensional imaging due to the cylindrical structure design of the hyperlens. In 2010, Rho *et al.* presented a spherical hyperlens for two-dimensional sub-diffraction-limited real-time imaging at visible frequencies.[30] Unlike the cylindrical hyperlens that uses the linearly p-polarized illumination, the spherical hyperlens uses the non-polarized illumination that stimulates transverse magnetic (TM) waves spanning the whole two-dimensional reciprocal space which follow the hyperbolic dispersion for two-dimensional super resolution imaging. In Rho *et al.*'s design, Ti_3O_5 (30 nm) with high dielectric permittivity was chosen to combine with Ag (as shown in Figs. 3(a)–3(b)) and two orthogonal dielectric permittivities with high contrast were achieved ($\varepsilon_r = -64 - 19.83\mathrm{i}$ and $\varepsilon_\theta = 0.42 - 0.11\mathrm{i}$). Although the transverse electric (TE) waves that follow the isotropic dispersion could be stimulated at the same time due to the non-polarized illumination, they can be filtered out due to the ultra-small value of ε_θ. At the same time, the anisotropic dispersion relation is ultra-flat over a large range of wave vectors, which makes TM waves with different values of k_θ propagate in the hyperlens along almost the same direction as shown in Fig. 3(c). The value of k_θ adiabatically decreases during the radial propagation and a subdiffraction object can be gradually magnified to surpass the resolution limit of a conventional microscope.[31] Figures 3(d)–3(f) show the magnified images of a sub-diffraction-limited object: three dots positioned triangularly with a feature size down to 160 nm, which is much smaller than the diffraction limit at the 410 nm recording wavelength. The typical diameter of a spherical hyperlens is about several micrometers. Consequently, it is difficult to place the real sample precisely in its working area. To promote the real application of two-

dimensional spherical hyperlens, in 2017, Byun *et al.*[32] and Lee *et al.*[33] demonstrated a nanoimprint method to fabricate a spherical hyperlens array. In their method, a mold for spherical hyperlens array substrate was first made. Then, the spherical hyperlens array could be easily fabricated by duplicating the substrate and depositing metal and dielectric layers on it. Their final device area increased up to 5 cm × 5 cm.

The cylindrical or spherical geometry of a hyperlens is essential for magnification and the true far-field imaging. However, hyperlenses with cylindrical or spherical curved geometry usually face practical difficulties in placing the real sample on their inner surface and also in achieving a large FOV. Consequently, the metamaterial of planer structure but still possessing the ability to magnify has aroused considerable interest.[34–37] In 2010, Ma and Liu proposed a theoretical design by combining a metamaterial slab supporting the propagation of high wave vectors and a plasmonic waveguide couplers which can compensate for the phase, thus forming a magnified image.[36,37] According to this model, in 2018, Li *et al.*[34,35] experimentally demonstrated a planner super resolution lens by cascading a metallic meander cavity structure or distributed Bragg reflectors with a plasmonic waveguide coupler.[34,35] Lateral resolution at ∼ 180 nm can be achieved at $\lambda = 640$ nm with this kind of configuration.

Although a hyperlens allows the far-field super-resolution imaging at one snap shot, there are still some bottlenecks in this kind of device. First, the magnification factor of the hyperlens, which directly relates to the resolution improvement, can be calculated simply by the ratio between the outer cylindrical or spherical radius and the inner radius. However, a thicker hyperlens will lead to lower transmission level and will therefore prolong the exposure time, which is essential for real time imaging. The tradeoff between magnification and imaging speed is not very preferable; for example, a current hyperlens with 2× magnification would require an exposure time of up to tens of seconds.[22] Second, the working wavelengths for most of devices are limited to UV or short visible range, which is harmful to biological samples. Third, the metal and dielectric layers need to be deposited alternately for many circles. The requirement for the nanoscale thickness and the very concentric shape is a little harsh for current nano-fabrication techniques.

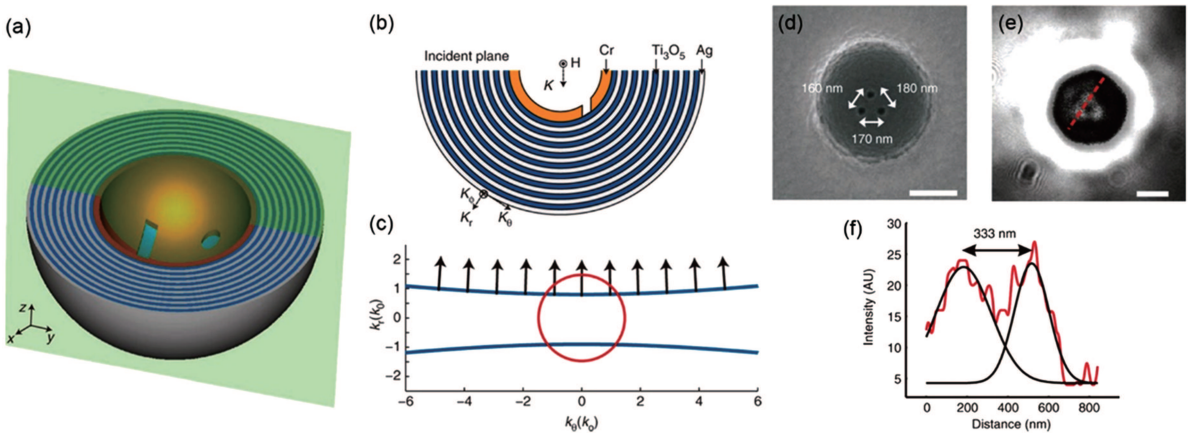


Fig. 3. (color online) Spherical hyperlens. (a) Schematic of spherical hyperlens comprised of 9 pairs of Ag and Ti_3O_5 layers. (b) Cross section of spherical hyperlens along green incident plane. The object with sub-wavelength features is carved in Cr layer atop Ag–Ti_3O_5 multilayer (also shown in light blue in (a)). TM component of unpolarized light relative to the plane is labelled by *K*. (c) Comparison between isofrequency contours for TM modes in hyperlens and isotropic medium made of silicon oxide. Arrows, which are of unit length and on ultra-flat curve, show that all the *k* components (including those much larger than the wave vectors available in dielectrics) propagate along the same radial direction, indicating the lack of diffraction. (d) SEM image of three dots positioned triangularly with gaps of 180 nm, 170 nm, and 160 nm. (e) Image and (f) intensity versus distance on cross section of the object along red line after being magnified. Reproduced with permission from Ref. [30].

2.2. Micro/nano-spheres with nano-jets

Due to the coupling of light to plasmons, there is always high intrinsic loss in the metallic-material-based hyperlens, which would limit their performance and practical applications. Compared with metallic devices, dielectric materials show much greater advantages due to their low loss and broadband transmission spectra which facilitate high-efficient and white light imaging. A macroscopic solid immersion dielectric lens (SIL) has been successfully demonstrated to improve the resolution of conventional optical imaging systems. However, the resolution improvement is limited to a factor of 2 in the visible spectrum due to the shortage of high-index lens materials and the large chromatic dispersion in the high-index materials.

The use of micro/nanoscale dielectric materials have brought new opportunities. Wavelength-scale SIL shows 25% improvement of the resolution compared with the macroscopic SIL.[38,39] Moreover in 2010, Wang *et al.*[40] presented a microsphere contacting technique for deep subdiffraction imaging.[40] They utilized ordinary glass to make microspheres (refractive index (RI) = 1.46; 2 μm < diameter (*D*) <

9 μm) to surpass the white-light diffraction limit and they achieved a resolution of 100 nm pitch size and a magnification between 4× and 8×. The experimental setup in transmission mode is shown in Fig. 4(a). The microspheres are placed on the top of the object surface, which is illuminated by a white-light halogen lamp source from another side. The microspheres collect the high spatial frequency information in the near field of the object and output propagating waves to a conventional objective lens. The super resolution imaging phenomenon is attributed to the fact that the micro/nanospheres can produce "nano-jects"; that is, the light can be focused on a hot spot with a subdiffraction size. Figures 4(b)–4(d) show the simulated cross-sectional intensity distributions for SIL, sphere, and sphere on metal surface with the same parameters (RI = 1.46; $D = 4.74$ μm; $\lambda = 600$ nm). The focus of the SIL with a truncated surface is still limited by the diffraction, whereas the intact spheres can form a subdiffraction focal spot and thus help to achieve subdiffraction imaging according to the reciprocal optics. Figure 4(e) shows the experimental results for a gold-coated fishnet anodic aluminum oxide (AAO) sample with a 100-nm periodic pitch. The structure was resolved clearly by using 4.74-μm-diameter microspheres. There is a tradeoff between resolution and FOV for microsphere contacting super-resolution imaging. According to the simulation, the super resolving ability shrinks with the increase of the microsphere diameter, which directly determines the FOV. Although the allowed largest diameter can be maximized to 30 μm at RI = 1.8, this value corresponds to a poor subdiffraction resolution. Consequently, the FOV is a significant challenge for this single microsphere contacting method.

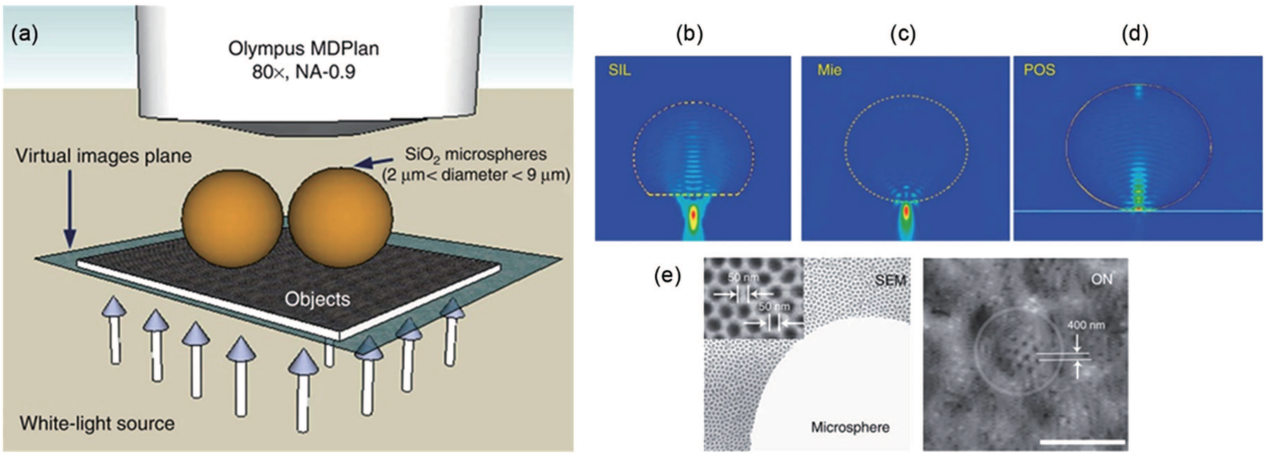


Fig. 4. (color online) Microsphere contacting nanoscope. (a) Schematic of transmission mode microsphere superlens integrated with classical optical microscope. Spheres collect near-field object information and form virtual images that can be captured by conventional lens. (b)–(d) Intensity distributions calculated for (b) SIL with height $H = D \times (1 + n^{-1})/2$, (c) sphere and (d) particle on surface of 40-nm-thick gold film, for the sphere with $D = 4.74$ μm and RI = 1.46 at $\lambda = 600$ nm. (e) Gold-coated fishnet AAO sample imaged with microsphere ($D = 4.74$ μm) superlens. Nanoscope clearly resolves pores of 100-nm-pitch (bottom left SEM image). Size of optical image between the pores within the image plane is 400 nm (bottom right ON image), which corresponds to magnification factor 8. Scale bar size: 5 μm. Reproduced with permission from Ref. [40].

In 2017, Fan *et al.*[41] proposed another method based on nano-sphere arrays to further increase the FOV without sacrificing the resolution.[41] They assembled visible-transparent, high-refractive-index, and deep-subwavelength-sized anatase TiO_2 nanoparticles ($D = 15$ nm; RI = 2.55) into a hemisphere or super-hemisphere shape similar to that of a conventional SIL as illustrated in Fig. 5(a). The nano-sphere assembled SIL is called all dielectric metamaterial SIL (mSIL) and is directly fabricated on the sample surface to collect the near-field high spatial frequency information in the following imaging process. Figures 5(b)–5(d) show the simulation results of electric field distribution in the medium when applying a 550-nm-wavelength plane wave illumination from the far field. Electric field confinements are observed in the gaps between nanoparticles, indicating the ability of the metamaterial media to modulate and confine visible light on a nanoscale. Because TiO_2 is nearly free of energy dissipation at visible wavelengths, this near-field coupling effect among neighboring nanoparticles can effectively propagate through the medium over long distances, forming an arrayed patterned illumination landscape on the surface of an underlying substrate (Fig. 5(c)). These illumination spots are evanescent in nature, containing high spatial frequency information. Their sizes are mainly determined by the size of TiO_2 nanoparticles, having a full width at half maximum (FWHM) resolution of ∼ 8 nm (Fig. 5(d)). Based on this mSIL contacting technique, periodic size of 100 nm on a raw integrated chip (Fig. 5(e)) and 90 nm on a gold covered integrated chip (Fig. 5(f)) were successfully resolved with an FOV around 500 μm^2.

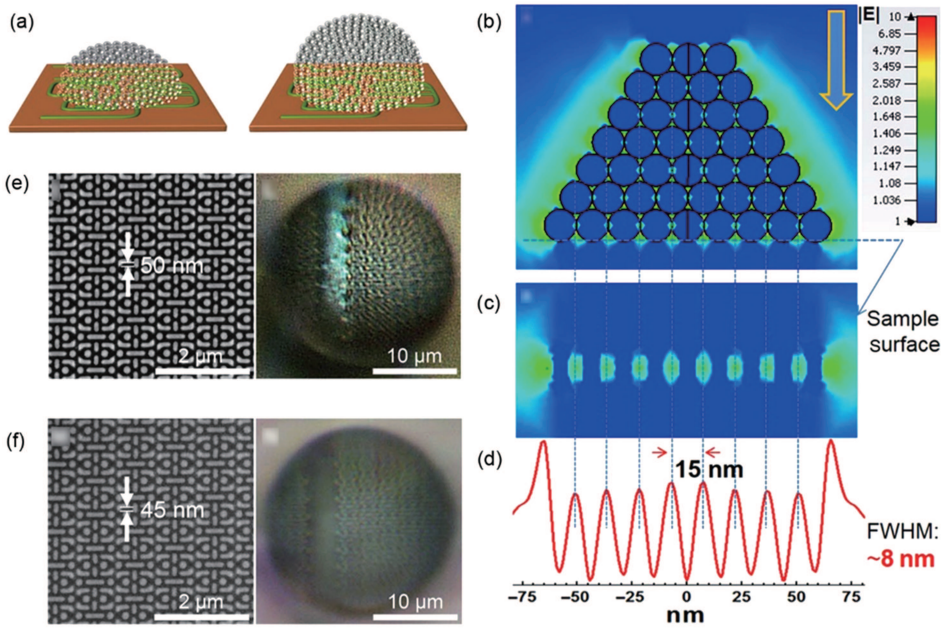


Fig. 5. (color online) All-dielectric TiO_2 mSIL. (a) Schematic of fabricated half-spherical and super-spherical mSIL. (b) Plane wave (λ = 550 nm) passing through the stacked TiO_2 nanoparticles. Electric field hot spots are generated in gaps between contacting particles, which guide light to the underlying sample. (c) Large-area nanoscale evanescent wave illumination that can be focused onto the sample surface because of the excitation of nano-gap mode. (d) Size of illumination spots, which is equal to particle size and has FWHM resolution of $\sim$ 8 nm. (e) SEM image of a wafer pattern with 100 nm pitch size and its optical microscopy image with TiO_2 mSIL with magnification factor 3.0. (f) SEM image of wafer pattern with 90 nm pitch size after being gold-coated and its optical microscopy image with TiO_2 mSIL with magnification factor 3.1. Reproduced with permission from Ref. [41].

The mSIL method can work at a wide visible spectrum, form a two-dimensional image, and is applicable for metal and non-metal samples. Theoretically, the mSIL could be designed to be very large to achieve a satisfactory FOV. However, the reported mSILs have diameters limited to 10–30 μm, probably because the fabrication method (nano-solid fluid assembly method) needs an absolute advantage of the interfacial tension with respect to the gravity for forming a regular sphere shape. Meanwhile, there is an aberration near the boundary of the mSIL (Figs. 5(e) and 5(f)), which could reduce the effective FOV.

2.3. High wave vector illumination with spatial frequency shift effect

Spatial frequency shift effect is very effective to detect the high spatial frequency information within a large area and thus achieve wide-field subdiffraction imaging. When the object is illuminated by light with spatially modulated intensity or phase, the spatial frequency spectrum of the object will shift with the incident spatial frequency, and this is expressed as

$$F_{\text{output}}(\boldsymbol{k}) = F_{\text{object}}(\boldsymbol{k} - \boldsymbol{k}_{\text{illumination}}), \tag{2}$$

where $\boldsymbol{k}_{\text{illumination}}$ is the spatial frequency domain vector of the illumination, $F_{\text{object}}(\boldsymbol{k})$ is the spatial frequency spectrum of the object under uniform illumination, and $F_{\text{output}}(\boldsymbol{k})$ is the output spatial frequency spectrum. The spatial frequency spectrum around $\boldsymbol{k}_{\text{illumination}}$ can be shifted to the center in the spatial frequency domain, and thus can be carried by the propagating wave for far-field detection. When $|\boldsymbol{k}_{\text{illumination}}| > 2\pi/\lambda$, the high frequencies corresponding to the subdiffraction spatial information of the object can be shifted into the passband of conventional objectives to enable super resolution imaging.

Structured illumination microscopy (SIM) is a favorite wide-field microscopy and the resolution is improved by a factor of two.[42] In SIM, two propagating waves interfere at the object plane and produce an intensity modulated illumination pattern. The sample is fluorophore labelled, and the high-resolution spatial information can be observed in the form of Moiré fringes. Because the illumination pattern formed by propagating wave is still limited by the diffraction, the best resolution that can be achieved by conventional SIM is $\lambda/4$NA.

To further increase the resolution, nano-structures are resorted to stimulate and propagate plasmonic waves to construct structured illumination.[7] In 2014, Wei *et al.*[43] experimentally demonstrated a plasmonic SIM (PSIM). The object was illuminated by the interference pattern formed by counter propagating surface plasmonic (SP) waves at the interface between a thin silver layer and a silica substrate. Due to the high wave vector of the SP wave, a 2.6-times resolution improvement was achieved. In 2017, Ponsetto *et al.*[2] demonstrated another localized PSIM (LPSIM), which can triple in resolution. In the experiment, a nano silver antenna array was fabricated to generate a localized plasmonic field array, which works as a structured pattern to illuminate the object. The resolution improvement is directly determined by the pitch of the metal antenna array, which cannot be finer than $\lambda/4$NA otherwise an undetectable gap would occur between the low spatial

frequency range and the shifted high spatial frequency range. To further increase the resolution, higher order SP illumination patterns and the dispersive property of the SP wave can be utilized in the future.

Although the conventional SIM has already shown potential in label-free microscopy,[44–46] all the reported super resolution PSIMs were only operated on the fluorescent-tagged samples. The reason can probably be attributed to the severe noise caused by the scattering from the nano-slits/nano-antennas, and to the deviation of the field distribution profile from a simple sine wave.

Evanescent wave illumination with pure and high transverse wave vector can be used to achieve label-free super resolution imaging. It is easy to excite large proportional evanescent waves around nano optical structures due to their natural small feature size on a wavelength scale and the devices based on nano-structures are usually more compact than the evanescent wave illumination based on total internal reflection.[47,48] In 2013, Hao *et al.*[49] used the surficial evanescent waves of a microfiber (diameter = 2.5 μm) to work as a near-field illumination source.[49] The microfiber was controlled by a piezoelectric positioning stage and simply placed on the sample surface. The $|\boldsymbol{k}_{\text{illumination}}|$ is proportional to the effective refractive index of the propagation mode in the microfiber. Based on the frequency shift effect, a slot pair structure of 225 nm central width was successfully resolved under 600-nm-wavelength evanescent wave illumination by using a 0.8 NA objective ($\lambda/\text{NA} = 750$ nm). However, the FOV is inevitably confined by the diameter of the microfiber, although it allows theoretically unlimited detection in the dimension along the microfiber. Moreover, it cannot be applied to two-dimensional super resolution imaging because one-dimensional microfiber guides the evanescent wave in a single direction and only enables one-dimensional spatial frequency shift.

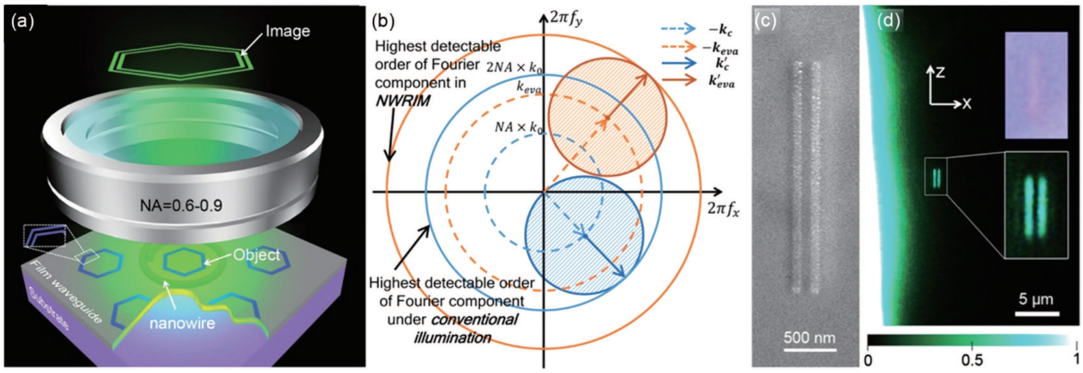


Fig. 6. (color online) Schematic of the NWRIM. (a) Schematic of configuration and imaging process. Hexagon array is used as an example object to show effect of NWRIM. Under omnidirectional evanescent illumination from fluorescent NWR, subdiffraction nested features of central hexagon show up in far-field image. (b) Basic mechanism of NWRIM method. $\boldsymbol{k}_{\text{c}}$ and $\boldsymbol{k}_{\text{c}}'$ are surficial wave vectors of the illuminating and scattered light, respectively, under conventional illumination. $\boldsymbol{k}_{\text{eva}}$ and $\boldsymbol{k}_{\text{eva}}'$ are surficial wave vectors of illuminating and scattered light, respectively, under NWR evanescent illumination. (c) SEM image of a line pair with spacing of 170 nm on Al_2O_3–SiO_2–Si double layer substrate. (d) Far-field optical microscopy image of slot pair under nanowire illumination. Images under nanowire illumination (lower inset) and conventional illumination (upper inset) are magnified for clarity. NA = 0.85. Reproduced with permission from Ref. [50].

In 2017, Liu *et al.* proposed a new on-chip evanescent illumination design to achieve label-free two-dimensional subdiffraction imaging with large FOV based on nano source active illumination.[50] This enables omnidirectional evanescent wave to propagate for two-dimensional imaging and its on-chip design makes it easily compatible with conventional microscope and other super resolution configurations. This method is called NWR illumination microscopy (NWRIM). Figure 6(a) shows the schematic of the NWRIM. A semiconductor NWR is placed on a subwavelength film waveguide, working as a localized nanoscale light source. When the NW is pumped, fluorescent light effectively couples to and propagates in the underlying film. Because of the nanoscale thickness of the film, a high proportion of the evanescent wave is distributed above the top surface during the light propagation. The objects on the film surface act as a perturbation to the propagating mode in the film waveguide, and the scattered light is collected by a far-field objective, contributing subdiffraction spatial information to the final image. Figure 6(b) shows the detectable spatial frequency components in NWRIM and in conventional microscopy, respectively. For conventional microscopy, the wave vectors of illumination and detection are both confined by the NA of the objective. Consequently, the far-field detectable Fourier components are limited to a circle with a radius of $2\text{NA} \times k_0$. While in NWRIM with an illumination wave vector of k_{eva}, the highest detectable Fourier components are expanded to $k_{\text{eva}} + \text{NA} \times k_0$, and a higher resolution can be achieved. The Stokes frequency shift between the NW's fluorescence and the pumping laser facilitates the filtering of the noise caused by the pumping laser to achieve a high signal-to-noise-ratio (SNR). Furthermore, the high luminescence efficiency and high mechanical flexibility of the semiconductor nanowires make this NWRIM efficient and reliable for subdiffraction imaging. Figure 6(d) shows

the optical microscopic image of a slot pair structure with a center-to-center distance of 170 nm, which is much smaller than the diffraction limited resolution ($\lambda/\mathrm{NA} = 611$ nm). This was clearly resolved under the evanescent illumination generated by a single fluorescent CdS nanowire (central fluorescent wavelength = 520 nm) plus a 200 nm thick Al_2O_3 film waveguide.

The NWRIM can detect the high spatial frequency information with large FOV and thus shows great potential on fast imaging. The FOV is directly related to the light propagation distance in the film waveguide. To improve the propagation distance and thus the FOV, Liu *et al.*[50] designed an Al_2O_3–SiO_2 double layer waveguide as shown in Fig. 7(a). The nanowire is placed on the surface of Al_2O_3, and its fluorescent light couples into the Al_2O_3 layer. The SiO_2 layer prevents the light from leaking into the Si substrate and enables a theoretical propagation distance above 100 μm (Fig. 7(b)). Pang *et al.*[51] also optimized the fabrication process of film waveguides by increasing the fabrication temperature for reducing the defect in the film and realizing a longer propagation distance experimentally (Fig. 7(c)). The current FOV achieved in NWRIM reaches ∼ 6000 μm^2 with 122 nm resolution.[51]

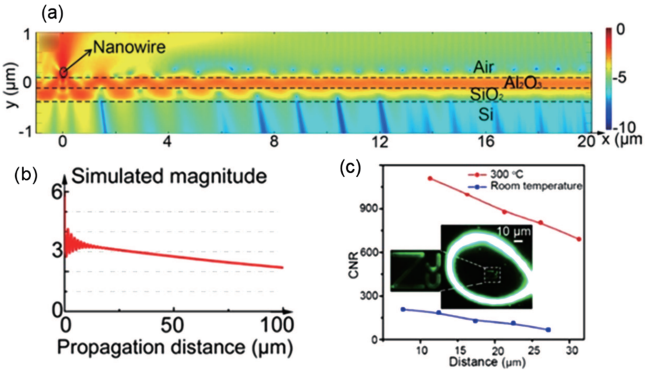


Fig. 7. (color online) FOV of NWRIM. (a) Simulated cross-sectional field distribution with fluorescent CdS nanowire on Al_2O_3–SiO_2–Si double layer substrate. Intensity is shown on a log scale. (b) Simulated field magnitude in Al_2O_3 film along propagation direction. (c) CNR of images of fabricated slot structures at different distances from fluorescent CdS nanowire light source, achieved with film waveguide fabricated at 300 °C and room temperature, respectively. Inset shows two-dimensional "ZJU" pattern illuminated by NWR. The area circled by NWR is ∼ 6000 μm^2. Reproduced with permission from Refs. [50] and [51].

The main parameters of the reported label-free, wide-field super resolution imaging methods are listed in Table 1. The NWRIM method achieves the largest FOV, which is 1–2 orders of magnitude larger than that of the other methods.

Table 1. Main parameters of recently reported wide-field label-free subdiffraction imaging methods.

Ref.	Material	Working spectrum	Resolution/nm	FOV/μm^2
[23]	cylindrical hyperlens	single wavelength	150	one-dimensional imaging
[30]	spherical hyperlens	single wavelength	160	∼ 10
[40]	microsphere	multiple wavelength	100 (metal)	∼ 10
[41]	mSIL	multiple wavelength	90 (metal), 100 (nonmetal)	∼ 500
[49]	nano fiber	multiple wavelength	150	one-dimensional imaging
[24]	non-resonant hyperlens	visible	250	one-dimensional imaging
[50], [51]	NWRIM	multiple wavelength	122	∼ 6000

The NWRIM is also a versatile method that is applicable to diverse sample types. Figures 8(a) and 8(b) show that the NWRIM was used to examine Blu-ray disks with 150 nm tracks. No storage structure is visible under conventional illumination in Fig. 8(a). In contrast, under NW illumination (Fig. 8(b)), grating-like structures in the blank region and storage dots in the recorded region are both apparently observed. Figures 8(c)–8(f) show that the NWRIM was used to image an integrated chip. In the dense areas of the integrated chip, the distances among the metal wires are very small, especially in the inner layers. Using NWRIM, all the closely arranged wires can be resolved (Fig. 8(d)), whereas under conventional illumination they are severely blurred. Figure 8(h) shows the image of an etched two-dimensional "ZJU" pattern on an Al_2O_3 film illuminated by a single fluorescent CdS NWR. The center-to-center feature size of 152 nm has been clearly resolved in the NWRIM image.

In NWRIM, the detectable spatial frequency information is shifted outwards from the origin in the spatial frequency domain to center at the spatial frequency domain vector of the evanescent illumination. The highest detectable spatial frequency components are extended, while at the same time the low spatial frequency information around the origin is lost, especially when the NA of the imaging objective is small. The loss of low frequency information could cause blur and aberration of the image. As shown in Figs. 9(a)–9(e), a V-type structure is clearly resolved at a diffraction limited region II but the image is blurred in the larger-sized region III. This problem can be tackled by combining together the low spatial frequency components detected at the conventional illumination and the high spatial frequency components provided by NWRIM. Because the camera in the far field only captures the intensity distribution and abandons the phase information, the spatial frequency spectrum cannot be achieved by a simple Fourier transform of the image. To recover the phase and thus enable the frequency domain to be spliced, the au-

thors resorted to a literature algorithm (Gerchberg–Saxton algorithm), in which an enough proportional overlap between the two neighboring sub-regions in the spatial frequency domain is required to recover the complex amplitude distribution of the image. To meet this condition, Liu *et al.*[50] proposed a multiple wavelength illumination method. According to this method, the $\boldsymbol{k}_{\text{illumination}}$—that is, the center of the detected spatial frequency range—is directly related to the wavelength. One thing to be noted is that for two-dimensional image reconstruction, the illumination direction should also be scanned, which can be achieved by stimulating different parts of the NWR. Figure 9(f) shows that the simulated reconstruction of the V-type structure has three wavelengths, 390 nm, 520 nm, and 720 nm. The blur region and the aberration caused by the loss of low-frequency information disappear in the reconstructed image. In the future experiments, the wavelength scanning can be achieved by using nanowires with a broad emission spectrum or introducing nonlinear effects and selecting out scattered light with different wavelengths by filters in the far field.

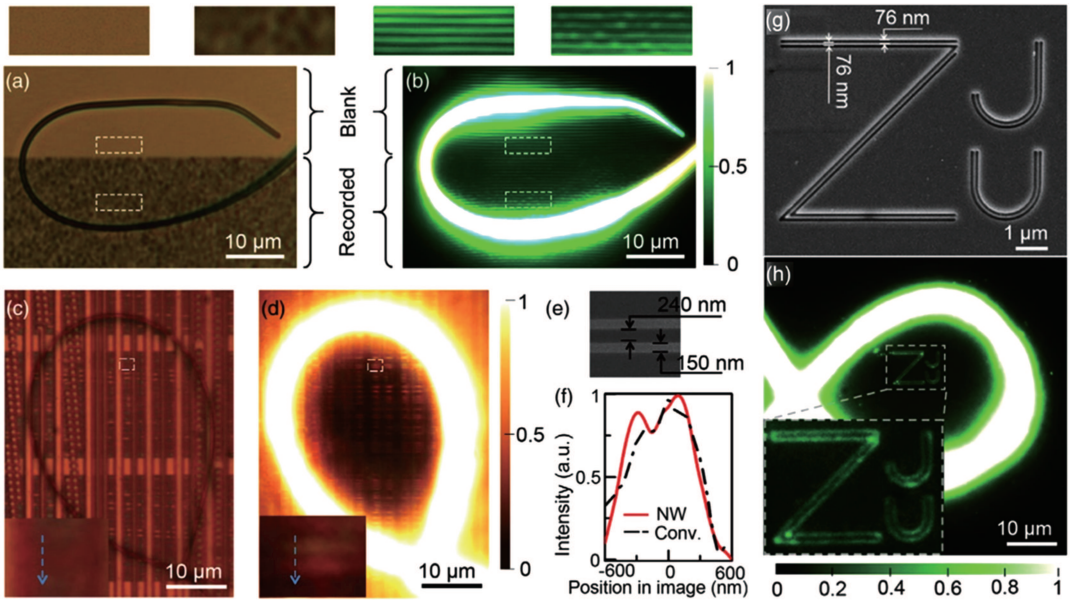


Fig. 8. (color online) NWRIM images of Blu-ray disk, integrated circuit, and "ZJU" pattern. (a) Conventional and (b) NWRIM images of Blu-ray disk. Boxed regions are magnified (top insets). (c) Conventional and (d) NWRIM images of integrated chip. Boxed regions are magnified (left bottom insets) and (e) SEM and (f) cross-sectional intensity distribution along the blue arrows. NWRIM and conventional illumination are denoted as NW and Conv., respectively. (g) SEM and (h) NWRIM images of arbitrary "ZJU" pattern etched on Al_2O_3 film. NA = 0.85. Reproduced with permission from Ref. [50].

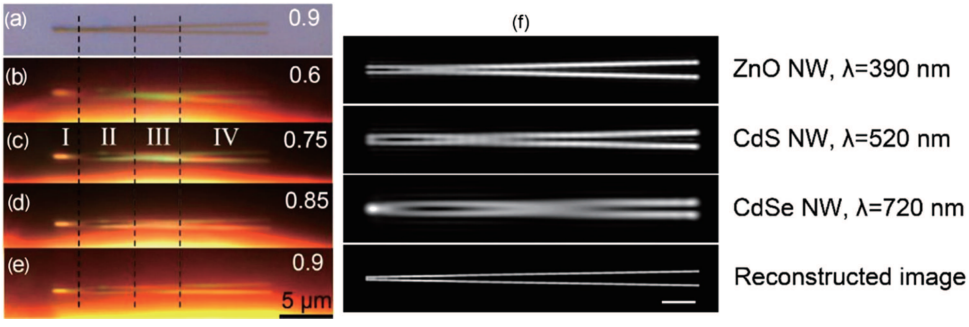


Fig. 9. (color online) Image reconstruction by multiple wavelength illumination. (a) Image of V-shaped structure (2° opening, 20 μm long) formed by 0.9 NA objective under conventional illumination. (b)–(e) Images of V-shaped structure under nanowire illumination formed by various standard objectives of NAs ranging from 0.6 to 0.9. (f) Image under evanescent wave illumination from nanowires of three different fluorescent wavelengths and reconstructed image. Scale bar size: 2 μm. Reproduced with permission from Ref. [50].

3. Conclusions and perspective

In this review paper, we have summarized the applications of novel nanostructures in label-free, wide-field super-resolution microscopy, including hyperlens, microsphere, mSIL, and NWRIM. The corresponding mechanism and experimental results of how to improve the resolution, SNR, and FOV have been analyzed. The key point in all these methods is to detect the high spatial frequency information of the objects, which is carried by normally decayed evanescent waves under conventional illumination. To interact with these evanes-

cent waves, the nanostructure-based-device has to be placed in the near field of the object, although the image can be projected to the far field. All these methods are limited to the surface detection without the ability to implement the deep three-dimensional imaging. Hyperlens, microspheres can couple the evanescent wave at the surface of the sample into propagating waves and form a super resolution image at one snap shot without needing any reconstruction. However, the SNR and FOV should be the main concern for hyperlens. Using gain materials but keeping the coherence in the hyperlens would be a potential solution. For the microsphere technique, it is difficult to observe a precise position and the FOV is also a tough problem. The NWRIM based on the frequency shift effect can detect the high spatial frequency information with a much wider FOV. However, for a complete spatial frequency components detection, many frames corresponding to different directions and shift values in the spatial frequency domain are required. The introduction of Galvo scanning system into the NW pumping system can increase the scanning speed and promise the real time wide-field label-free super resolution imaging.

References

[1] Kner P, Chhun B B, Griffis E R, Winoto L and Gustafsson M G L 2009 *Nat. Methods* **6** 339
[2] Ponsetto J L, Bezryadina A, Wei F, Onishi K, Shen H, Huang E, Ferrari L, Ma Q, Zou Y and Liu Z 2017 *ACS Nano* **11** 5344
[3] Schneider J, Zahn J, Maglione M, Sigrist S J, Marquard J, Chojnacki J, Krausslich H G, Sahl S J, Engelhardt J and Hell S W 2015 *Nat. Methods* **12** 827
[4] Kawata S, Inouye Y and Verma P 2009 *Nat. Photon.* **3** 388
[5] Liu X, Wong T T W, Shi J, Ma J, Yang Q and Wang L V 2018 *Opt. Lett.* **43** 947
[6] Wilson T 2011 *J. Microsc.* **244** 113
[7] Wei F and Liu Z 2010 *Nano. Lett.* **10** 2531
[8] Klar T A, Jakobs S, Dyba M, Egner A and Hell S W 2000 *Proc. Natl. Acad. Sci. USA* **97** 8206
[9] Rittweger E, Han K Y, Irvine S E, Eggeling C and Hell S W 2009 *Nat. Photon.* **3** 144
[10] Betzig E 1995 *Opt. Lett.* **20** 237
[11] Betzig E, Patterson G H, Sougrat R, Lindwasser O W, Olenych S, Bonifacino J S, Davidson M W, LippincottSchwartz J and Hess H F 2006 *Science* **313** 1642
[12] Dickson R M, Cubitt A B, Tsien R Y and Moerner W E 1997 *Nature* **388** 355
[13] Zhuang X 2009 *Nat. Photon.* **3** 365
[14] Diezmann A v, Shechtman Y and Moerner W E 2017 *Chem. Rev.* **117** 7244
[15] Hecht B, Sick B, Wild U P, Deckert V, Zenobi R, Martin O J F and Pohl D W 2000 *J. Chem. Phys.* **112** 7761
[16] Wang L and Xu X G 2015 *Nat. Commun.* **6** 8973
[17] Ma D D D, Lee C S, Au F C K, Tong S Y and Lee S T 2003 *Science* **299** 1874
[18] Tong L, Gattass R R, Ashcom J B, He S, Lou J, Shen M, Maxwell I and Mazur E 2003 *Nature* **426** 816
[19] Law M, Greene L E, Johnson J C, Saykally R and Yang P 2005 *Nat. Mater.* **4** 455
[20] Kolmakov A, Zhang Y, Cheng G and Moskovits M 2003 *Adv. Mater.* **15** 997
[21] Choi M, Lee S H, Kim Y, Kang S B, Shin J, Kwak M H, Kang K Y, Lee Y H, Park N and Min B 2011 *Nature* **470** 369
[22] Lee H, Liu Z, Xiong Y, Sun C and Zhang X 2007 *Opt. Express* **15** 15886
[23] Liu Z, Lee H, Xiong Y, Sun C and Zhang X 2007 *Science* **315** 1686
[24] Sun J, Shalaev M I and Litchinitser N M 2015 *Nat. Commun.* **6** 7201
[25] Jacob Z, Alekseyev L V and Narimanov E 2006 *Opt. Express* **14** 8247
[26] Jacob Z, Alekseyev L V and Narimanov E 2007 *J. Opt. Soc. Am. A* **24** A52
[27] Kildishev A V and Narimanov E E 2007 *Opt. Lett.* **32** 3432
[28] Zhang W, Chen H and Moser H O 2011 *Appl. Phys. Lett.* **98** 073501
[29] Smith E J, Liu Z, Mei Y F and Schmidt O G 2009 *Appl. Phys. Lett.* **95** 083104
[30] Rho J, Ye Z, Xiong Y, Yin X, Liu Z, Choi H, Bartal G and Zhang X 2010 *Nat. Commun.* **1** 143
[31] Cang H, Salandrino A, Wang Y and Zhang X 2015 *Nat. Commun.* **6** 7942
[32] Byun M, Lee D, Kim M, Kim Y, Kim K, Ok J G, Rho J and Lee H 2017 *Sci. Rep.* **7** 46314
[33] Lee D, Kim Y D, Kim M, So S, Choi H J, Mun J, Nguyen D M, Badloe T, Ok J G, Kim K, Lee H and Rho J 2018 *ACS Photon.* **5** 2549
[34] Li H, Fu L, Frenner K and Osten W 2018 *Opt. Express* **26** 10888
[35] Li H, Fu L, Frenner K and Osten W 2018 *Opt. Express* **26** 19574
[36] Ma C and Liu Z 2010 *Appl. Phys. Lett.* **96** 183103
[37] Ma C and Liu Z 2011 *J. NanoPhoton.* **5** 051604
[38] Mason D R, Jouravlev M V and Kim K S 2010 *Opt. Lett.* **35** 2007
[39] Lee J Y, Hong B H, Kim W Y, Min S K, Kim Y, Jouravlev M V, Bose R, Kim K S, Hwang I C, Kaufman L J, Wong C W, Kim P and Kim K S 2009 *Nature* **460** 498
[40] Wang Z, Guo W, Li L, Luk'yanchuk B, Khan A, Liu Z, Chen Z and Hong M 2011 *Nat. Commun.* **2** 218
[41] Fan W, Yan B, Wang Z and Wu L 2016 *Sci. Adv.* **2** e1600901
[42] Gustafsson M G L 2000 *J. Microsc.* **198** 82
[43] Wei F, Lu D, Shen H, Wan W, Ponsetto J L, Huang E and Liu Z 2014 *Nano. Lett.* **14** 4634
[44] Chowdhury S, Dhalla A H and Izatt J 2012 *Biomed. Opt. Express* **3** 1841
[45] Chowdhury S, Eldridge W J, Wax A and Izatt J A 2017 *Biomed. Opt. Express* **8** 2496
[46] Chowdhury S, Eldridge W J, Wax A and Izatt J 2017 *Optica* **4** 537
[47] Hao X, Kuang C, Li Y and Liu X 2013 *Opt. Lett.* **38** 2455
[48] Olshausen P v and Rohrbach A 2013 *Opt. Lett.* **38** 4066
[49] Hao X, Liu X, Kuang C, Li Y, Ku Y, Zhang H, Li H and Tong L 2013 *Appl. Phys. Lett.* **102** 013104
[50] Liu X, Kuang C, Hao X, Pang C, Xu P, Li H, Liu Y, Yu C, Xu Y, Nan D, Shen W, Fang Y, He L, Liu X and Yang Q 2017 *Phy. Rev. Lett.* **118** 076101
[51] Pang C, Liu X, Zhuge M, Liu X, Somekh M G, Zhao Y, Jin D, Shen W, Li H, Wu L, Wang C, Kuang C and Yang Q 2017 *Opt. Lett.* **42** 4569